



LUND UNIVERSITY

A computer program for the analysis of timber structures exposed to fire

Fredlund, Bertil

1985

[Link to publication](#)

Citation for published version (APA):

Fredlund, B. (1985). *A computer program for the analysis of timber structures exposed to fire*. (LUTVDG/TVBB--3020--SE; Vol. 3020). Division of Building Fire Safety and Technology, Lund Institute of Technology.

Total number of authors:

1

General rights

Unless other specific re-use rights are stated the following general rights apply:

Copyright and moral rights for the publications made accessible in the public portal are retained by the authors and/or other copyright owners and it is a condition of accessing publications that users recognise and abide by the legal requirements associated with these rights.

- Users may download and print one copy of any publication from the public portal for the purpose of private study or research.
- You may not further distribute the material or use it for any profit-making activity or commercial gain
- You may freely distribute the URL identifying the publication in the public portal

Read more about Creative commons licenses: <https://creativecommons.org/licenses/>

Take down policy

If you believe that this document breaches copyright please contact us providing details, and we will remove access to the work immediately and investigate your claim.

LUND UNIVERSITY

PO Box 117
221 00 Lund
+46 46-222 00 00

LUND INSTITUTE OF TECHNOLOGY · LUND · SWEDEN
DIVISION OF BUILDING FIRE SAFETY AND TECHNOLOGY
REPORT LUTVDG/(TVBB - 3020)
ISSN 0282 - 3756

BERTIL FREDLUND

A COMPUTER PROGRAM FOR THE
ANALYSIS OF TIMBER STRUCTURES
EXPOSED TO FIRE

LUND 1985

LUND INSTITUTE OF TECHNOLOGY

Division of Building Fire Safety and Technology

Box 118

S-221 00 LUND, Sweden

Telephone: +46-46-107360

Report LUTV0G/(TVBB-3020)(1985)

ISSN 0282-3756

Bertil Fredlund

A COMPUTER PROGRAM FOR THE ANALYSIS
OF TIMBER STRUCTURES EXPOSED TO FIRE

Translated by

L J Gruber BSc(Eng) MICE MISTructE

CONTENTS	PAGE
1 INTRODUCTION	1
2 HEAT TRANSFER ANALYSIS	3
2.1 Conservation of energy	3
2.2 Conservation of mass	4
2.3 Initial and boundary conditions	4
2.4 The effect of mass flow rate on the convective surface coefficient of heat transfer	7
2.5 The kinetics of wood pyrolysis and the variation in material properties	10
3 FINITE ELEMENT APPROXIMATION	12
3.1 Solution procedure	12
3.2 Finite element discretisation	12
3.3 Matrix formulation of the energy balance equations	13
3.4 Conductivity matrix	14
3.5 Convective matrix	15
3.6 Heat capacity matrix	15
3.7 Internally generated heat	16
3.8 Heat flow at the boundary	17
3.9 Integration with respect to time and critical time increments	19
4 COMPUTER PROGRAM	21
4.1 Background	21
4.2 Subroutines	21
4.3 Input data	24
4.4 Example of required input data	25

5	COMPARISON OF EXPERIMENTS AND CALCULATIONS	28
5.1	The material used in the comparisons	28
5.2	Test on a wooden cube exposed to radiation	29
5.3	Test on a glued laminated timber beam according to ISO 834	35
5.4	Sensitivity analysis of thermal properties	39
6	SUMMARY AND CONCLUSIONS	44

1 INTRODUCTION

Theoretical analysis of the pyrolysis of wood implies that a non-linear heat balance equation must be solved. Since there are no analytical solutions in existence for this complex nonlinear problem, the only way of tackling it is to use numerical methods such as the finite difference or finite element method.

In (1), Wickström describes a computer program, TASEF-2, based on the finite element method for the analysis of the thermal response of structural elements when exposed to the action of fire. These structural elements may consist of several materials and may contain cavities. The heat flow at the boundaries may comprise radiation and convection. An explicit forward difference method is used which means that latent heat, for instance in conjunction with the vaporisation of water in concrete, can be taken into consideration. The program is two dimensional.

On the basis of a model developed by the author for the pyrolysis of wood (2), a computer program, WOOD1, is presented in this report. The program is one-dimensional and is based on the finite element method. The solution techniques are based on those described in (1).

Expressions which must be specially introduced in conjunction with the pyrolysis of wood are those for the pyrolytic reaction in the wood material and the consumption of charcoal at the surface of the material. This means that a mathematical description of these two reactions must be provided.

The reaction is assumed to conform to a first order Arrhenius function. As a result of the reaction in the wood material, its density gradually decreases. This means that expressions must be introduced for the thermal properties of partially pyrolysed wood. The volatile

pyrolysis products give rise to an internal convective heat flow and modify the convective coefficient of heat transfer at the surface of the material. The convective flow gives rise to a nonsymmetric convection matrix.

Owing to consumption of charcoal at the surface of the material, the mesh division at the boundaries must be successively changed during the calculations.

The report presents the theoretical model and describes the way in which it can be approximated by the finite element method. A brief description is given of the subroutines in the program. Finally, experiments and calculations are compared, and a sensitivity analysis of the thermal properties of wood is carried out.

2. HEAT TRANSFER ANALYSIS

2.1 Conservation of energy

The fundamental heat flow equation for one-dimensional thermal conduction and internal convection in a material is

$$\frac{\partial}{\partial x} k \frac{\partial T}{\partial x} - \kappa \frac{\partial T}{\partial x} + Q - \rho c \frac{\partial T}{\partial t} = 0 \quad (2.1)$$

where

k = conductivity, W/mK

κ = convective term, W/m²K

Q = heat generated internally per unit volume, J/m³

ρ = density, kg/m³

c = specific heat capacity, J/kgK

T = temperature, K

x = positional coordinate, m

t = time, s

The convective term is defined as

$$\kappa = c_{pg} \dot{m}'' \quad (2.2)$$

where

c_{pg} = specific heat capacity of volatile pyrolysis products, J/kgK

\dot{m}'' = mass flow rate per unit area and time, kg/m²s

In the above, the fundamental assumption is that for each x there is local thermodynamic equilibrium, i.e. that the solid phase and the gaseous phase in the material have the same temperature over a small space about x .

2.2 Conservation of mass

If the momentum equation is not taken into consideration, the expression for conservation of mass is

$$\frac{\partial \dot{m}''}{\partial x} = \frac{\partial \rho}{\partial t} \quad (2.3)$$

The simplification implies that the volatile pyrolysis products can move about freely in the solid phase and that pressure gradients or the velocity of the pyrolysis products cannot be calculated.

In actual fact, the assumption that the volatile pyrolysis products can move freely within the solid phase conflicts with the fundamental assumption that there is local thermodynamic equilibrium. Thermodynamic equilibrium between the phases implies that these are in good thermal contact.

2.3 Initial and boundary conditions

In order that Equation (2.1) may be solved, the boundary and initial conditions must be specified. The initial conditions are given by the initial temperature distribution in the solid phase at the reference time zero. The boundary conditions are given as prescribed energy flow rates or temperatures at the boundaries.

The energy flow rate at the boundary must satisfy the heat balance equation

$$q_n = -nk \frac{\partial T}{\partial x} \quad (2.4)$$

where

n = normal directed outwards from the boundary

q_n = prescribed flow rate at the boundary

It is assumed that at a free boundary there are four energy flows, namely

- convection between the solid phase and the surrounding gas
- radiation between the solid phase and the surrounding gas
- energy of chemical reaction at the surface of the material
- outward movement of volatile pyrolysis products.

All these are complex phenomena, and only approximate relationships can therefore be given. It is assumed that the convective term conforms to the expression

$$q_n^c = h(T_s - T_g) \quad (2.5)$$

where

q_n^c = heat transfer by convection, W/m^2

h = surface coefficient of heat transfer, W/m^2K

T_s = surface temperature, K

T_g = ambient gas temperature, K

Radiation from the surface of the material is approximated by

$$q_n^r = \epsilon_r \sigma (T_s^4 - T_g^4) \quad (2.6)$$

where

q_n^r = heat transfer by radiation, W/m^2

ϵ_r = resultant emissivity

σ = Stefan-Boltzmann constant

T_s = absolute surface temperature, K

T_g = absolute gas temperature, K

The resultant emissivity varies with surface characteristics and geometry. In fire engineering applications, radiant heat transfer takes place between the surrounding flames and the surface of the material. A common assumption is to calculate the resultant emissivity as that between two infinitely long parallel planes (3)

$$\epsilon_r = \frac{1}{1/\epsilon_s + 1/\epsilon_g - 1} \quad (2.7)$$

where

ϵ_s = emissivity of surface

ϵ_g = emissivity of gas

The energy of chemical reaction at the surface is given by

$$q_n^{ch} = n \Delta H_s \cdot \dot{s} \quad (2.8)$$

where

$-\Delta H_s$ = heat generated by the reaction at the surface, J/kg

\dot{s} = rate of recession of material surface due to the reaction,
m/s

It is assumed that the chemical reaction at the surface is described by a curve according to the following empirical equation (4)

$$\dot{s} = T_s \beta e^{-(E_A/RT_s)} \quad (2.9)$$

where

T_s = surface temperature, K

β = empirical constant, 1/sK

E_A = activation energy, J/mol

R = universal gas constant, J/mol K

The energy flow rate at the surface of the material due to the emitted volatile pyrolysis products is given by

$$q_n^{mf} = n \kappa_s (T_s - T_0) \quad (2.10)$$

where

κ_s = convective term according to Equation (2.2) at the surface of the material

T_0 = reference temperature at time $t = 0$

The total heat flow rate is calculated by summing the flow rates due to convection, radiation, surface reactions and mass flow

$$q_n = q_n^c + q_n^r + q_n^{ch} + q_n^{mf} \quad (2.11)$$

2.4 The effect of mass flow rate on the convective surface coefficient of heat transfer

The products of pyrolysis given off at the surface of the material influence the convective surface heat transfer conditions. Owing to emission of the volatile pyrolysis products in the boundary layer, the temperature gradient across the boundary layer is no longer linear.

If the conductivity of the gas in the boundary layer is denoted k_g and $\kappa = \dot{m}'' c_p$ for the volatile pyrolysis products emitted at the surface of the material, a heat balance equation for the boundary layer can be written as

$$k_g \frac{\partial^2 T}{\partial x^2} + \kappa \frac{\partial T}{\partial x} = 0 \quad (2.12)$$

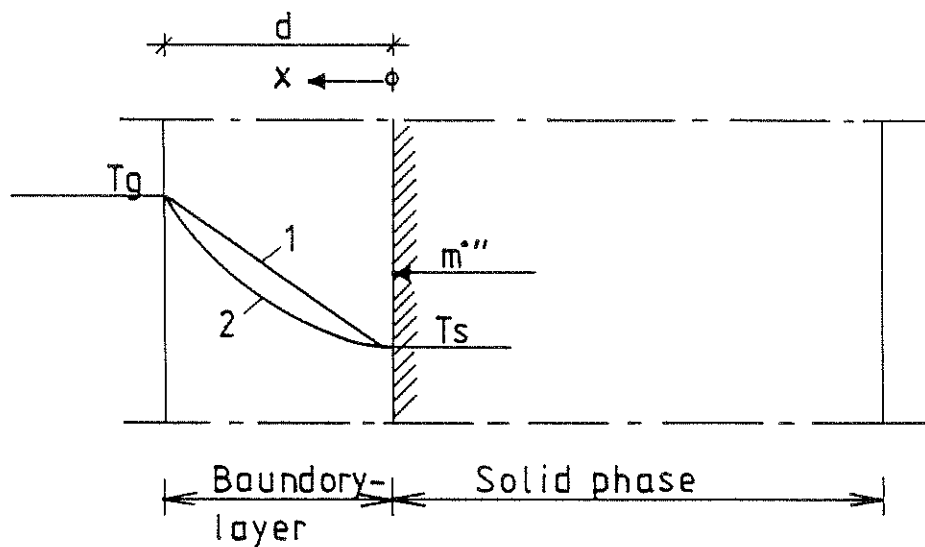


FIG. 2.1. Temperature distribution across a boundary layer adjacent to the surface of a material. Curve 1) applies when there are no volatile pyrolysis products emitted from the solid phase, and Curve 2) when pyrolysis products are being emitted.

The solution of this differential equation is

$$T = C_1 e^{r_1 x} + C_2 e^{r_2 x}$$

with $r_1 = 0$

$$r_2 = \kappa/k_g$$

If the thickness of the boundary layer is denoted d , the constants C_1 and C_2 can be calculated by considering that (see FIG. 2.1)

$$T = T_s \text{ when } x = 0$$

$$T = T_g \text{ when } x = d.$$

With the values of the constants C_1 and C_2 substituted, the temperature distribution across the boundary layer is given by

$$T(x) = T_s - \frac{T_g - T_s}{\frac{\kappa}{k_g} - 1} \left(1 - e^{-\frac{\kappa}{k_g} x} \right) \quad (2.13)$$

The temperature gradient adjacent to the surface of the material is obtained by differentiating Equation (2.13) with respect to x and substituting the coordinate for the material surface, i.e. $x = 0$.

When volatile pyrolysis products are being emitted, the temperature gradient at the surface of the material, with the surface coefficient of heat transfer defined by $h = k_g/d$, will be

$$\left(\frac{dT}{dx} \right)_{x=0} = \frac{\kappa}{hd} \left(\frac{1}{e^{\kappa/h} - 1} \right) (T_g - T_s) \quad (2.14)$$

When temperature distribution across the boundary layer is linear, the temperature gradient at the surface of the material is

$$\left(\frac{dT}{dx} \right)_{x=0} = \frac{1}{d} (T_g - T_s) \quad (2.15)$$

Heat transfer at the surface of the material is proportional to the temperature gradient at the surface. The usual convective energy transfer across a boundary layer can be corrected with respect to mass transfer across the boundary layer by the introduction of the blowing factor $E(b)$ which is defined as the ratio of Equation (2.14) to Equation (2.15), as given by

$$E(b) = \frac{\kappa}{h} \left(\frac{1}{e^{\kappa/h} - 1} \right) \quad (2.16)$$

The convective heat transfer between the solid phase and the surrounding gas is then

$$q_n^c = h(T_s - T_g) E(b) \quad (2.17)$$

For small values of κ/h , i.e. a small mass flow rate at the surface of the material, the function $E(b)$ approaches 1 while for large values of κ/h it approaches zero.

2.5 The kinetics of wood pyrolysis and the variation in material properties

A number of complex chemical reactions are involved in the pyrolysis of wood. The process of pyrolysis is assumed to conform to a mean reaction described by an Arrhenius function

$$\frac{\partial \rho}{\partial t} = -\rho b e^{-(E_A/RT)} \quad (2.18)$$

where

E_A = activation energy, J/mol

R = universal gas constant, J/mol K

b = constant, 1/s

ρ = density at section x at time t , kg/m³

The original wood material is assumed to be divided into an irreducible part 2 which produces charcoal that is oxidised at the surface of the material, and an active part 1 which produces volatile pyrolysis products. In terms of densities, this gives

$$\rho = \rho_1 + \rho_2 \quad (2.19)$$

The specific heat capacity of the wood material is assumed to follow a linear variation with the enthalpy for the constituent materials 1 and 2 which gives the following function of the density

$$c_p = \frac{\rho_0}{\rho} \left(\frac{\rho - \rho_2}{\rho_0 - \rho_2} \right) c_{p0} + \frac{\rho_2}{\rho} \left(\frac{\rho_0 - \rho}{\rho_0 - \rho_2} \right) c_{p2} \quad (2.20)$$

where

c_{p0} = specific heat capacity of wood material, J/kg K

c_{p2} = specific heat capacity of charcoal, J/kg K

c_p = specific heat capacity at section x at time t , J/kg K

ρ = density at section x at time t , kg/m³

ρ_0 = density of original wood material, kg/m³

ρ_2 = density of charcoal, kg/m³

Thermal conductivity is assumed to be given by a linear variation of the densities of the constituent materials

$$k = \left(\frac{\rho - \rho_2}{\rho_0 - \rho_2} \right) k_0 + \left(\frac{\rho_0 - \rho}{\rho_0 - \rho_2} \right) k_2 \quad (2.21)$$

where

k = thermal conductivity at section x at time t , W/mK

k_0 = thermal conductivity of original wood material, W/mK

k_2 = thermal conductivity of charcoal, W/mK

3. FINITE ELEMENT APPROXIMATION

3.1 Solution procedure

The heat balance equations set out in Chapter 2 contain nonlinear boundary conditions and material properties which vary with temperature and density. Analytical solutions are available only for linear applications of simple geometries and with simple boundary conditions. The only way in which a solution can be obtained is therefore a numerical method. The method decided on in this case, which can be easily expanded so as to apply to more than one dimension, is the finite element method. The presentation below is based on the one-dimensional case.

3.2 Finite element discretisation

The finite element method is characterised by the studied continuum being divided into small subregions, finite elements. These elements may vary in size and shape. Inside each element the temperature is approximated with the aid of the temperature at certain points of contact between the elements, i.e. the nodes.

Inside each element the temperature field is approximated by a shape function in such a way that the temperature inside the element is described only by means of the nodal temperatures. A polynomial is usually chosen as the approximation function. For the one-dimensional case the temperature is approximated as

$$T(x) = \sum_i^n N_i \bar{T}_i = \underline{N} \bar{\underline{T}} \quad (3.1)$$

where \bar{T}_i is the temperature at node i , n the number of degrees of freedom or nodal temperatures per element, and N_i the shape function.

The shape functions N_i are chosen in such a way that they assume the value 1 at node i and are zero at all other nodes. In the elements in contact with node i , N_i assumes values between zero and one. In all the other elements the function is zero.

3.3 Matrix formulation of the energy balance equations

By introduction of the symbols $\nabla = \frac{\partial}{\partial x}$ and $\bar{\nabla} = \frac{\partial}{\partial t}$, the governing differential equation in (2.1) can be written as

$$\nabla(k\nabla T) - \kappa\nabla T + Q - \rho c \bar{\nabla} T = 0 \quad (3.2)$$

Equation (3.2) is changed into weak formulation by multiplication by the weighting function v and integration over the volume V .

$$\int_V [v[\nabla(k\nabla T) - \kappa\nabla T + Q - \rho c \bar{\nabla} T]] dV = 0 \quad (3.3)$$

Partial integration of the first term, using Green's formula, produces

$$\int_V \nabla v (k\nabla T) dV + \int_V v \kappa \nabla T dV + \int_V v \rho c \bar{\nabla} T dV - \int_V v Q dV - \int_S v n k \nabla T dS = 0 \quad (3.4)$$

where n is the outward normal at boundary S .

The weighting function v is selected according to Galerkin's method in which the weighting function is put equal to the shape function N , i.e.

$$v = \tilde{N}^T \quad (3.5)$$

For a one-dimensional element with two degrees of freedom whose length is ΔL , the simplest shape function is

$$\tilde{N} = [N_1 \ N_2] = \left[1 - \frac{x}{\Delta L} \quad \frac{x}{\Delta L} \right] \quad (3.6)$$

The last integral in Equation (3.4) contains the boundary condition according to Equation (2.4). Substitution of (2.4), (3.1) and (3.5) into (3.4) produces

$$\int_{\tilde{V}} \tilde{\nabla N}^T (k \tilde{\nabla N}) d\tilde{V} + \int_{\tilde{V}} \tilde{N}^T k \tilde{\nabla N} d\tilde{V} + \int_{\tilde{V}} \tilde{N}^T \rho c \tilde{N} d\tilde{V} - \int_{\tilde{V}} \tilde{N}^T Q d\tilde{V} + \int_{\tilde{S}} \tilde{N}^T q_n d\tilde{S} = 0 \quad (3.7)$$

It is easiest to perform integration separately for each element, after which the contributions of all elements are assembled into global matrices. If the material properties are assumed constant in each element, the integrations in Equation (3.7) can be carried out analytically.

3.4 Conductivity matrix

For a one-dimensional internal element of length ΔL , the first integral in Equation (3.7) is calculated.

The derivatives $\tilde{\nabla N}^T$ and $\tilde{\nabla N}$ are obtained as

$$\tilde{\nabla N}^T = \begin{bmatrix} -1/\Delta L \\ 1/\Delta L \end{bmatrix} \quad (3.8)$$

and

$$\tilde{\nabla N} = [-1/\Delta L \quad 1/\Delta L] \quad (3.9)$$

With Equations (3.8) and (3.9) substituted, the local conductivity matrix is calculated by simple integration

$$\tilde{K}^k = \int_0^{\Delta L} \tilde{\nabla N}^T (k \tilde{\nabla N}) A dx = \frac{Ak}{\Delta L} \begin{bmatrix} 1 & -1 \\ -1 & 1 \end{bmatrix} \quad (3.10)$$

where A is the cross sectional area of the element.

Since conductivity generally varies as a function of temperature and density, that value of k is used which is valid for the mean temperature and mean density of an element.

3.5 Convective matrix

The second integral in Equation (3.7) which contains the contribution due to the internal mass flow is calculated in the same way as for the conductivity matrices. Substitution of \underline{N}^T and $\nabla \underline{N}$ according to Equations (3.6) and (3.9) and integration over the element length ΔL produces

$$\underline{K}^K = \int_0^{\Delta L} \underline{N}^T \kappa \nabla \underline{N} dV = \frac{A\kappa}{2} \begin{bmatrix} -1 & 1 \\ -1 & 1 \end{bmatrix} \quad (3.11)$$

Note that the convective matrix is not symmetric. Owing to this complication, the whole matrix must be stored in the computer. In the case of symmetric matrices, the entire matrix is not normally stored. If the mass flow rate is large, the convective term also gives rise to numerical difficulties. There are however methods available to prevent numerical instability. These are based on a nonlinear form of the shape function (5).

3.6 Heat capacity matrix

The heat capacity matrix is calculated from the third integral in Equation (3.7). Substitution of \underline{N}^T and \underline{N} and integration over the length of the element produces

$$\underline{C} = \int_0^{\Delta L} \underline{N}^T \rho c \underline{N} dx = \frac{A\rho c \Delta L}{6} \begin{bmatrix} 2 & 1 \\ 1 & 2 \end{bmatrix} \quad (3.12)$$

This matrix can however be simplified into a lumped diagonal matrix without any loss of computational accuracy (1). Owing to this simplification, when the change in energy content for node i has been calculated for a time increment, the associated change in temperature can be easily computed. See Section 3.9.

The simplified heat capacity matrix can be written as

$$\underline{C} = \frac{A\rho c\Delta L}{2} \begin{bmatrix} 1 & 0 \\ 0 & 1 \end{bmatrix} \quad (3.12)$$

3.7 Internally generated heat

The heat generated inside the element is calculated from the fourth integral in Equation (3.7). Substitution of \underline{N}^T and integration over the length of the element produces

$$\underline{F}^Q = \int_0^{\Delta L} \underline{N}^T Q dV = \frac{AQ\Delta L}{2} \begin{bmatrix} 1 \\ 1 \end{bmatrix} \quad (3.13)$$

The energy released per unit volume is a function of the rate of pyrolysis. If the rate of reaction is denoted $\dot{\Delta H}$, the energy released can be calculated from

$$Q = \Delta H \dot{\rho} \quad (3.14)$$

where $\dot{\rho}$ conforms to an Arrhenius function according to Equation (2.18).

3.6 Heat flow at the boundary

The last integral in Equation (3.7) represents the boundary conditions. For the case where the heat flow at the boundary is prescribed, the nodal flow rate can be calculated by substituting Equation (2.11) into the integral, which produces

$$\int_S \tilde{N}^T q_n dS = \int_S \tilde{N}^T (q_n^c + q_n^r + q_n^{ch} + q_n^{mf}) dS \quad (3.15)$$

If the contribution of radiation to the heat transfer layer, defined as

$$h_r = \epsilon_r \sigma \frac{(T_s^4 - T_g^4)}{T_s - T_g} \quad (3.16)$$

is introduced, the heat flow at the boundary due to radiation, according to Equation (2.6), can be re-written as

$$q_n^r = h_r (T_s - T_g) \quad (3.17)$$

In the same way as for the thermal conductivity matrix and the convective matrix, values of h_r corresponding to the actual temperature levels are substituted during the calculations. In this case h_r is calculated according to Equation (3.16) using temperatures from the previous calculation stage.

Substitution of Equations (2.17), (3.17), (2.8) and (2.10) into Equation (3.15) yields

$$\begin{aligned} \int_S \tilde{N}^T q_n dS &= \int_S \tilde{N}^T (hE(b) + h_r + n\kappa_s) \tilde{N} dS + \int_S \tilde{N}^T (hE(b) + h_r + n\kappa_s) T_g dS + \\ &+ \int_S \tilde{N}^T n \Delta H_s \dot{s} ds \end{aligned} \quad (3.18)$$

The three surface integrals in Equation (3.18) are calculated for the surface elements. For the one-dimensional case there are two boundaries, namely for $x = 0$ and $x = L$. These integrals are solved easily since integration is carried out over the surfaces at the boundaries where the shape function has the value 1. The solution is exemplified for the edge element at node $x = 0$.

The first term in Equation (3.18) is denoted $\underline{K}^q \underline{T}$ and, with the values substituted, is

$$\underline{K}^q \underline{T} = A(hE(b) + h_r + n\kappa_s) \begin{bmatrix} 1 & 0 \\ 0 & 0 \end{bmatrix} \underline{T} \quad (3.19)$$

and if the other two terms in Equation (3.18) are denoted \underline{F}^q , we have

$$\underline{F}^q = A[(hE(b) + h_r + n\kappa_s)T_g - n\Delta H_s \dot{s}] \begin{bmatrix} 1 \\ 0 \end{bmatrix} \quad (3.20)$$

We can now, with the above notations, summarise Equation (3.7) by the following equation

$$(\underline{K}^k + \underline{K}^k + \underline{K}^q) \underline{T} + \underline{C} \bar{v} \underline{T} = \underline{F}^Q + \underline{F}^q \quad (3.21)$$

where the sum of \underline{K}^k , \underline{K}^k and \underline{K}^q constitutes the total heat transfer matrix \underline{K} , i.e. the stiffness matrix. \underline{C} is the simplified lumped heat capacity matrix. The right hand side consists of the external imposed heat flow \underline{F}^q and the internally produced heat \underline{F}^Q . The total heat load is denoted \underline{F} .

3.9 Integration with respect to time and critical time increments

The heat balance equation is solved incrementally by the forward difference method. This means that the solution does not converge if the time increment is greater than a critical value Δt_{cr} . The magnitude of the critical time increment is a function of the element size, material quantities and boundary conditions. An example of the other factors which govern the size of the time increment is that it must bear a reasonable relationship to variations in material quantities and changes in boundary conditions (1).

When the simplified heat capacity matrix with only diagonal elements according to Equation (3.12) is used, the new temperature for time $t+\Delta t$ can be calculated without solving a system of equations for all nodes. The method is therefore explicit.

If the energy content or enthalpy is defined as

$$\underline{E} = \underline{C} \underline{T} \quad (3.22)$$

Equation (3.21) can be re-written as

$$\underline{K} \underline{\bar{T}} + \underline{\bar{V}} \underline{E} = \underline{F} \quad (3.23)$$

The explicit forward difference formula can, with the aid of Equation (3.23), be written as

$$\underline{E}_{t+\Delta t} = \underline{E}_t + (\underline{F}_t - \underline{K}_t \underline{T}_t) \Delta t \quad (3.24)$$

where t is the time and Δt the time increment.

The new temperature $\underline{T}_{t+\Delta t}$ is then calculated directly from Equation (3.22).

According to (1), the critical time increment Δt_{cr} can be approximated by the following expression

$$\Delta t_{cr} = \min \left(\frac{C_{ii}}{K_{ii} + \frac{1}{2} \sum_j K_{Fij}} \right) \quad (3.25)$$

where

$$K_{Fij} = \frac{dF_i}{dT_j} \quad \text{and } i \text{ and } j \text{ denote rows and columns respectively.}$$

It is evident from the equation that when the ratio of heat capacity to conductivity is small, the time increment is small.

Normally it is the boundary nodes which are critical with respect to the time increment because of their high surface coefficient of heat transfer, but even elements in the pyrolysis zone may, depending on the rate of pyrolysis, exert a decisive influence.

4. COMPUTER PROGRAM

4.1 Background

The computer program WOOD1 has been developed on the lines of the presentation in Chapters 1 and 2. All subroutines are programmed in FORTRAN 77. The subroutines have been developed for one-dimensional heat flow and assume dry wood. With some modifications, the program can be expanded so as to hold for two dimensional heat flow and for wet wood. In the simplified case, expansion to permit calculations with the inclusion of a moisture content is based on modification of the heat capacity matrix and the energy content of the gases evolved during pyrolysis.

Some subroutines were originally written by Ulf Wickström, and are represented by one-dimensional versions of the routines in the computer program TASEF-2.

4.2 Subroutines

FIG. 4.1 presents an outline of the subroutines in WOOD1 and the way these are linked to one another.

The following is a brief description of the subroutines.

<u>Subroutine</u>	<u>Description</u>
AFFE	Calculates the radiative component of the surface coefficient of heat transfer
ASSA1	Calculates the global thermal conductivity matrix
ASSK1	Calculates the convective terms of the nodes
ASSP1	Calculates the global heat capacity matrix

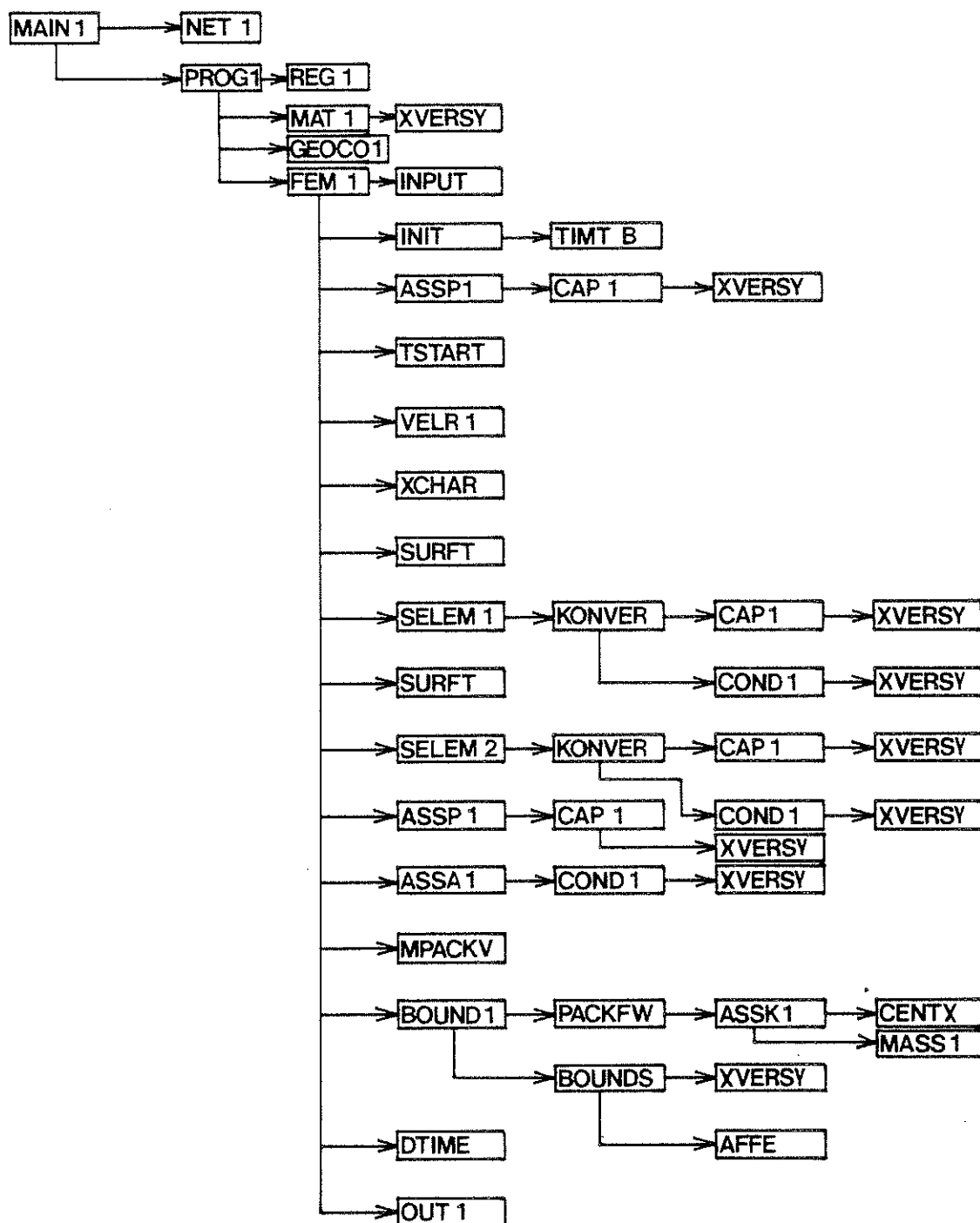


FIG. 4.1. The subroutines in the program WOOD1 and the relationships between these.

<u>Subroutine</u>	<u>Description</u>
BOUND1	Summates energy flows to the nodes. The component flows are convection in the material, energy from the pyrolysis process, and contributions from the boundaries
BOUNDS	Calculates the total heat transfer at the material surfaces
CAP1	Calculates the heat capacity of the nodes
CENTX	Calculates the coordinate x_c for the section where, for $x < x_c$, the pyrolysis gases flow towards boundary 1 and, for $x > x_c$, flow towards boundary 2
COND1	Gives the thermal conductivity of the elements
DTIME1	Calculates the critical time increment
FEM1	Main routine for the incremental procedure
GEOCO1	Assigns geometrical constants to the elements
INIT1	Initiates the temperature field in the solid phase
INPUT	Reads printout times
KONVER	Calculates the properties of boundary elements with respect to heat capacity and conductivity before mesh division at the boundary is updated
MAIN1	Determines maximum field sizes
MASS1	Calculates the contribution of each element to mass flow
MAT1	Reads physical input data for the constituent materials
MPACKV	Calculates heat flow due to thermal conductivity at each node
NET1	Creates computation network with the read geometrical data
OUT1	Writes output data for the times specified in input data
PACKFW	Calculates convective heat flow in the material
PROG1	Determines field sizes required for the current computational task
REG1	Calculates the region to which a certain element is assigned

<u>Subroutine</u>	<u>Description</u>
SELEM1	Indicates when computation network is to be changed by aggregating the two elements nearest to boundary 1
SELEM2	The same as SELEM1 but for boundary 2
SURFT	Calculates rate of reaction \dot{s} at the boundaries
TIMTB	Checks whether several computational cases are to be analysed. Reads input data such as compartment temperature as a function of time for the two boundaries
TSTART	Gives the first time increment
VELRI	Calculates rate of pyrolysis $\dot{\rho}$
XCHAR	Gives the coordinate of the pyrolysis zone.

4.3 Input data

Input data for the program WOOD1 are of the following types:

- Geometrical input data used for the generation of a computation network
- Material data are to be given for the constituent materials, pyrolysis gases, charcoal and the original wood material. For charcoal and wood the specific heat capacity and thermal conductivity are given as a function of temperature, and for the pyrolysis gases only the specific heat capacity is given as a function of temperature
- Kinetic input data for the pyrolytic reaction and the reactions at the surface are given. The density of the material in the pyrolysis zone is also specified to define the depth of penetration of the charred zone

- Input data which describe printout times.
- Boundary conditions for boundaries 1 and 2 are given in terms of the fire gas temperature as a function of time
- Conditional reading and simulation of several computational cases.

An example of input data for a simulation is given below. Explanatory comments are also given.

4.4 Example of required input data for the program WOOD1

```

1  F
2  .80 .010 1 30 F
3  .002 .004 .006 .008 .010 .012 .014 .016 .018 .020 .022 .024 .026 .028 .030
4  .032 .034 .036 .038 .040 .042 .044 .046 .048 .050 .052 .054 .056 .058 .060
5  DRY WOOD
6  10 1.
7  500. 150.
8  300.
9  5 0 . .15 50. .15 100. .15 200. .15 2000. .15
10 2 0. .0.05 2000. .0.05
11 3 0. 700. 1000. 900. 2000. 1100.
12 3 0. 1000. 1000. 5000. 2000. 5000.
13 5 0. 1000. 500. 1117. 1000. 1200. 1500. 1263. 2000. 1409.
14 0.50E-7 1. 3.1E3
15 1500. 63000. 8.314
16 2 0. 0. 2000. 0.
17 0.
18 F
19 13 1.1

```

```

20 .06 .067 0.1 .2 .30 .40 .50 .60 .70 .80 .90 1.0 1.1
21 F F 1
22 TEST EXAMPLE
23 1
24 5
25 0. 20. .03333 846. .3333 903. .7333 916. 10. 916.

```

Comments

1. TRUE if the program is to be run interactively
2. Total thickness (m), element thickness (m), number of material types, number of extra nodes.
TRUE if axysymmetric case.
3. Coordinates of extra nodes (m)
4. Coordinates of extra nodes (m)
5. Material name
6. >1 if material properties main region 1, cross sectional area (m²)
7. Density wood, density charcoal (kg/m³)
8. Density of pyrolysis zone for which depth of charring is defined (kg/m³)
9. Number of ordered pairs, temperature-conductivity ordered pair for wood (°C, W/mK)
10. Number of ordered pairs, temperature-conductivity ordered pair for charcoal (°C, W/mK)
11. Number of ordered pairs, temperature-specific heat capacity ordered pair for charcoal (°C, J/kg K)
12. Number of ordered pairs, temperature-specific heat capacity ordered pair for wood (°C, J/kg K)
13. Number of ordered pairs, temperature-specific heat capacity ordered pair for pyrolysis gas (°C, J/kg K)
14. $\beta_1, \beta_2, \beta_3$ where $\dot{s} = \beta_1 T_s \beta_2 \exp(-\beta_3/T_s)$ describes the reactions at the surface of the material (1/sK, -, K)
15. b, E_A, R where $\dot{\rho} = \rho b \exp(-E_A/RT)$ describes the rate of pyrolysis (1/s, J/mole, J/mole K)

16. Number of ordered pairs, temperature-energy consumed in surface reaction ($^{\circ}\text{C}$, J/kg)
17. Energy consumed during pyrolysis (J/kg)
18. TRUE if input data for printout times are given in minutes
19. Number of printout times, maximum simulation time (-, h or min)
20. Printout times (h or min)
21. TRUE if same temperature curve at both boundaries, TRUE if prescribed heat flow at boundary 2, number of simulation cases
- 21b. The prescribed heat flow at boundary 2 is given here if this is wanted according to previous input data line (W/m^2)
22. Heading for simulation, max. 80 characters
23. Counter
24. Number of time-gas temperature ordered pairs
25. Time-gas temperature ordered pair (h, $^{\circ}\text{C}$)

5 COMPARISON OF EXPERIMENTS AND CALCULATIONS

5.1 The material used in the comparisons

The accuracy of the computer program can be tested in relation to analytical solutions or experiments. Since there are no exact analytical solutions available for the problem studied here, such a comparison cannot be carried out. Even comparison with experiments is difficult since the investigations reported in the literature often omit input data which are important for simulation. However, a large number of fire tests on beams and columns, in most cases in conformity with standard fire tests according to ISO 834, have been reported. (6), (7), (8) and (9).

A detailed analysis of the behaviour of wood when exposed to the action of fire is given in (10). The report contains details of experiments, and describes the construction and solution of energy balance equations by computerised methods. The experiments and simulations described in the report are however relatively short, a few minutes. This is however natural since the report is largely concerned with ignition and fire spread.

Even if detailed information is available concerning experiments, uncertainties remain regarding boundary conditions, for instance combustion of the emitted volatile pyrolysis products just outside the surface of the material, or the extent of cracking in the charcoal layer. Generally speaking, there is a shortage of relevant knowledge concerning the thermal properties of wood and charcoal at high temperatures. To this must be added the uncertainty reported in the literature concerning determination of the kinetic constants. See, for instance, the table on p. 1.9 in (11) or p. 4-51 in (10). It is evident from these tables that there are at least as many values of the constants quoted as there are authors. The decision

taken in this report has been to test the kinetic constants in the literature against my own tests and then to study the sensitivity of some material constants.

5.2 Test on a wooden cube exposed to radiation

The test specimen was a wooden cube of 150 mm sides. Temperature sensors and thermocouples as well as resistive moisture sensors were installed in the cube at a spacing of 10 mm, initially at a distance of 2 mm from the surface exposed to radiation. The sides at right angles to the one exposed were insulated in order to simulate one-dimensional thermal radiation. These sides were also coated with a vapour barrier.

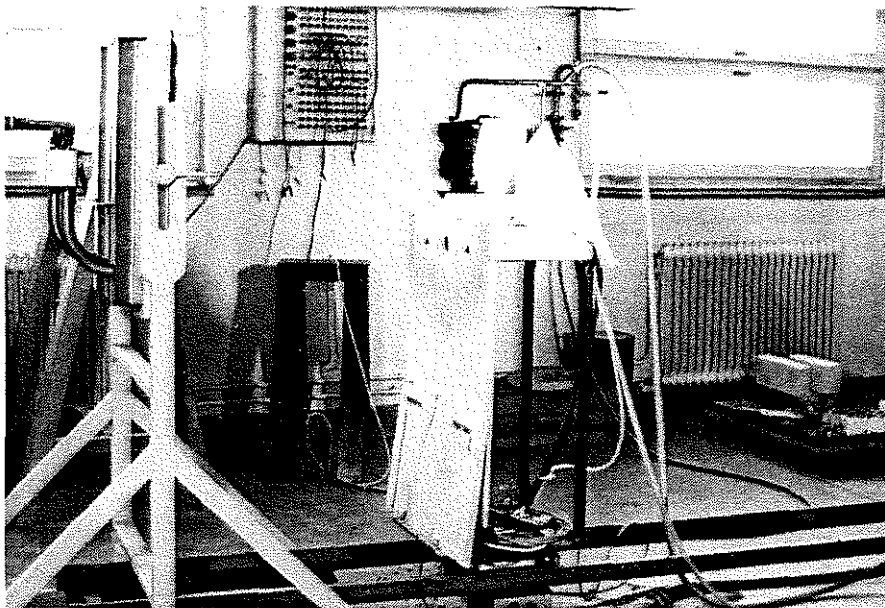


FIG. 5.1. Test arrangement for wooden cube exposed to radiation.

The specimen was mounted on a trolley in order to permit automatic distance adjustment from a computerised data collection system. A radiation meter was mounted near the wooden cube to measure the radiation incident on the cube. The source of radiation was a ceramic gas fired radiant panel of 350x350 mm. The test was carried out with the specimen in a normal room atmosphere.

The test arrangement is illustrated in FIG. 5.1. The measured incident radiation on the specimen is shown in FIG. 5.2, and the recorded temperature and moisture distribution as a function of time are shown in FIG. 5.3 and 5.4 respectively.

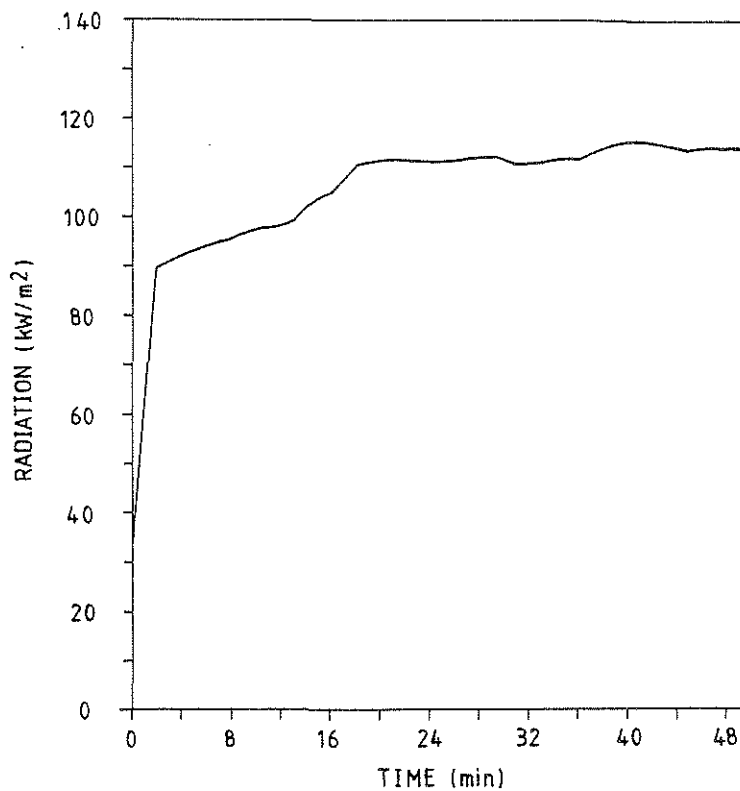


FIG. 5.2. Radiation incident on the specimen as a function of time.

$$\rho_{\text{dry}} = 455 \text{ kg/m}^3.$$

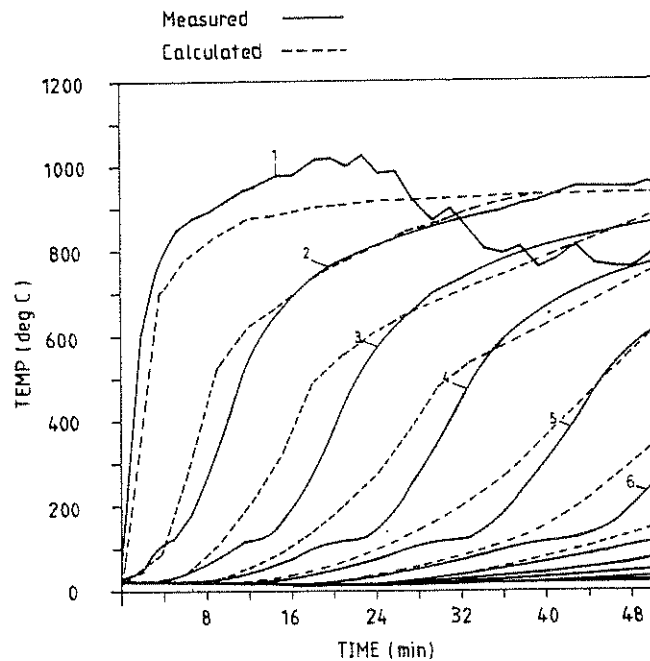


FIG. 5.3. Recorded and calculated temperature rise as a function of time at different distances from that side of the wooden cube which is exposed to radiation. $\rho_{\text{dry}} = 455 \text{ kg/m}^3$.

The depth of penetration of the charcoal layer was measured manually with the aid of three approx. 3 mm thick wood sticks inserted into the cube. The observed depth of charring is set out in FIG. 5.5.

The thickness of the charcoal layer can also be determined approximately from FIG. 5.3 by interpreting the shapes of the temperature curves at 900-1000°C. When the thermocouples inserted into the wood material are exposed at the material surface owing to combustion of the charcoal, they are affected by fluctuations in the gas temperature just outside the surface of the charcoal layer. On the assumption that

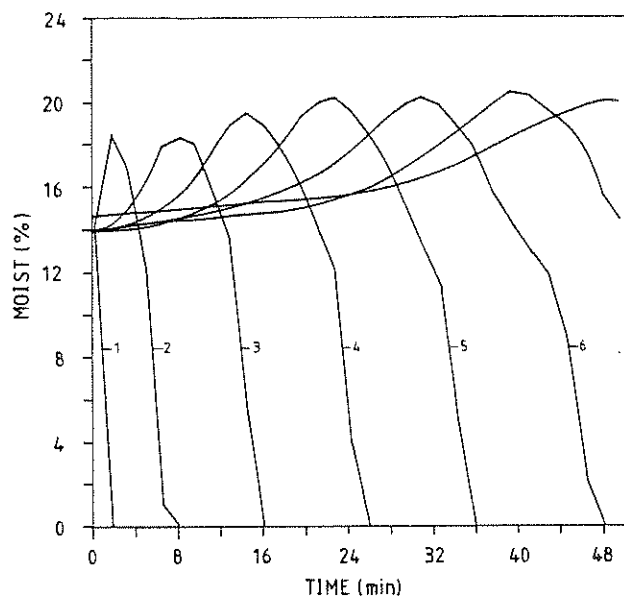


FIG. 5.4. Moisture distribution as a function of time in a wooden cube exposed to radiation. $\rho_{\text{dry}} = 455 \text{ kg/m}^3$

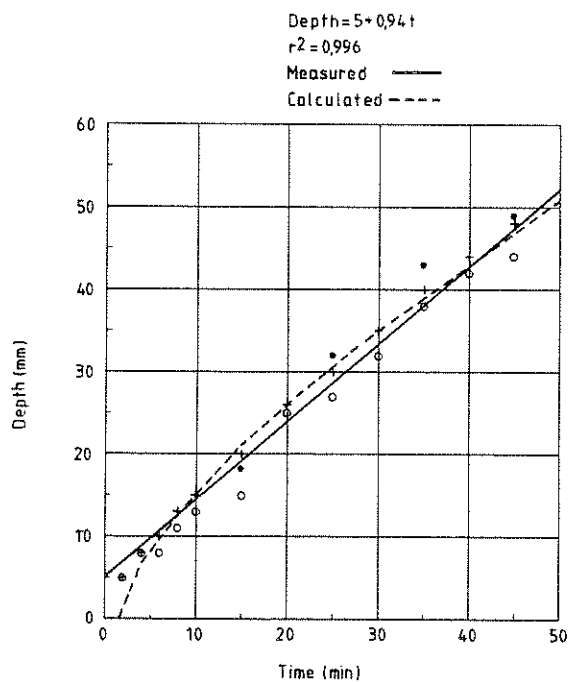


FIG. 5.5. Experimentally and theoretically determined depth of charring as a function of time in a wooden cube exposed to radiation. $\rho_{\text{dry}} = 455 \text{ kg/m}^3$

the position of the charcoal surface is determined by the occurrence of these fluctuations at each node, we have

Time min	Position of surface mm	Position of pyrolysis zone mm	Thickness of charcoal layer mm
14	2	18	16
36	12	40	28

The wooden cube exposed to radiation was simulated by the program WOOD1 using input data according to Table 5.1. The boundary conditions on the surface exposed to fire were represented by a fire gas temperature corresponding to incident radiation on the material surface according to the curve in FIG. 5.2. The opposite material surface was in contact with a constant air temperature of 20°C.

Table 5.1. Material data for simulation of wooden cube exposed to radiation

Density, wood	455		kg/m ³		
Density, carbon	150		kg/m ³		
Density which defines position of pyrolysis zone	300		kg/m ³		
Conductivity, wood	0.12		W/m K		
Conductivity, carbon	20, 0.05	400, 0.05	600, 0.20	1000, 0.40	W/m K
Specific heat capacity, wood	20, 1400	500, 1500		°C, J/kg K	
Specific heat capacity, carbon	20, 700	1000, 1000		°C, J/kg K	
Specific heat capacity, pyrolysis gas (as for air)	20, 1000	500, 1117	1000, 1200	°C, J/kg K	
Reaction constants for material surface					
β_1	$0.5 \cdot 10^{-6}$			1/s K	
β_2	1			-	
β_3	3100			K	

Table 5.1. (continued)

Heat of reaction for surface	0	J/kg
Reaction constants for pyrolysis		
b	1500	1/s
E_A	63000	J/mole
Heat of reaction for pyrolysis	0	J/kg

Owing to the convergence requirement, the length of the element was made only 2 mm. For surface elements on the side exposed to fire, the element length successively decreases as the material surface burns. When the surface element has decreased to $0.3\Delta L$, it is ignored in calculations and the boundary conditions are applied to the adjacent element.

In FIG. 5.3 and 5.5 the calculated temperature distribution and depth of charring have been shown by dashed lines.

Since the simulations were made on the assumption that the wood material is dry, there is a difference between the measured and calculated temperature distributions due to vaporisation of water at 100°C . When the wood has dried out, the curves in FIG. 5.3 are in good agreement but are displaced laterally by an amount corresponding to the time taken for vaporisation.

It is evident from FIG. 5.5 that the simulated depth of charring is in good agreement with that measured experimentally. The comparison shows how important it is to take account in the model of the water content of wood. One way in which this can be done is to represent

the vaporisation process by an Arrhenius function, with the heat of reaction equal to the heat of vaporisation. The constants in Table 5.1 were not selected specially in order to fit the calculations to the measured data, but are examples of values reported in the literature.

5.3 Test on a glued laminated timber beam according to ISO 834

At the request of the Norwegian Institute of Wood Technology, five glued laminated timber beams with bolts and fittings were tested at the Norwegian Fire Research Laboratory (Commission No 250103.00178). The firm Moelven Limtre A/S mounted extra temperature and moisture sensors in the beams in order to enable the author to carry out detailed measurements in addition to those specified in the commission to the Fire Research Laboratory.

FIG. 5.6 shows the gas temperature measured in the furnace as a function of time according to measurements at the Laboratory, and FIG. 5.7 shows the placing of the extra sensors.

One half of the cross section was simulated, with the boundary condition at one boundary in conformity with the measured furnace temperature, and that at the other boundary with a prescribed edge flow equal to zero. The reason for the zero edge flow is that the centre line is considered to be a line of symmetry.

The measured and calculated temperature fields as a function of time are compared in FIG. 5.8. The significance of the moisture ratio of wood is evident in this case also.

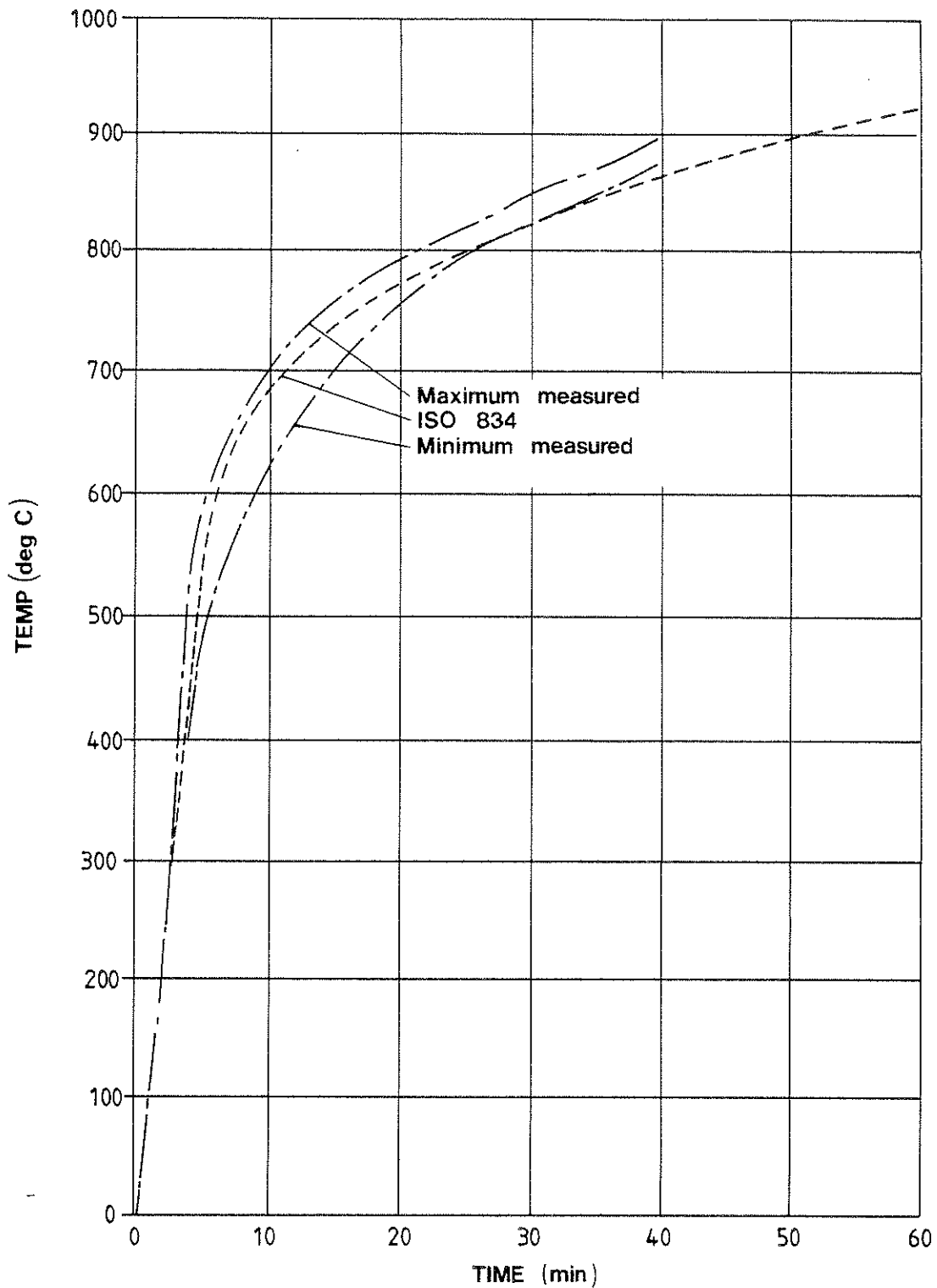


FIG. 5.6. Measured gas temperature-time curve for test on a glued laminated timber beam.

Beam 3	laminate no	Moisture content
	— " — 12	— " — 9,0 %
	— " — 11	— " — 10,5 %
	— " — 10	— " — 10,8 %
	— " — 9	— " — 11,0 %
	— " — 8	— " — 10,2 %
	— " — 7	— " — 10,8 %
	— " — 6	— " — 10,5 %
	— " — 5	— " — 11,8 %
	— " — 4	— " — 11,2 %
	— " — 3	— " — 9,5 %
	— " — 2	— " — 11,0 %
	— " — 1	— " — 11,1 %

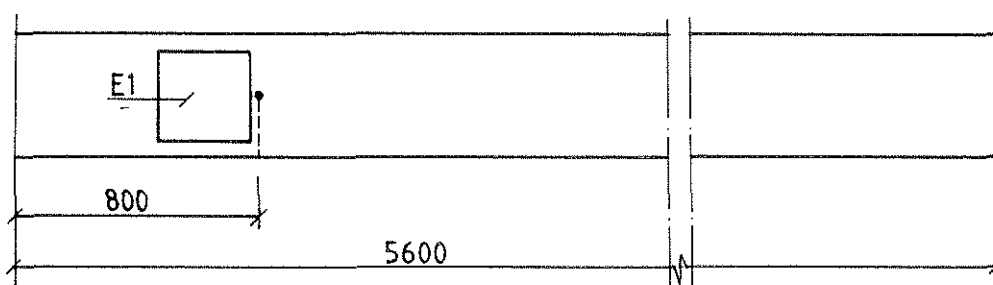
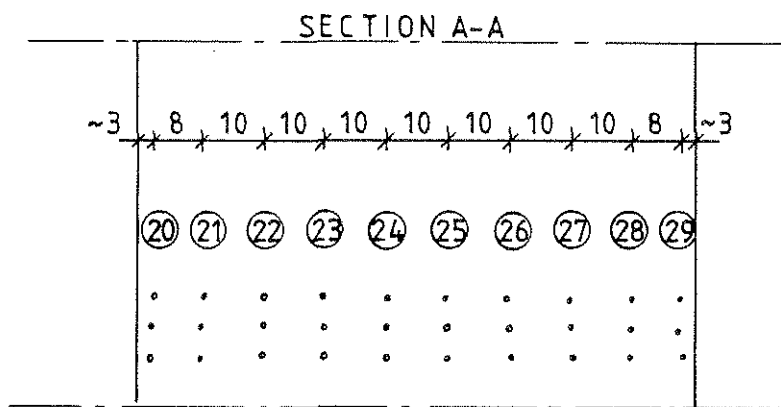


FIG. 5.7. Placing of temperature and moisture sensors in the glued laminated timber beam, and measured moisture ratios

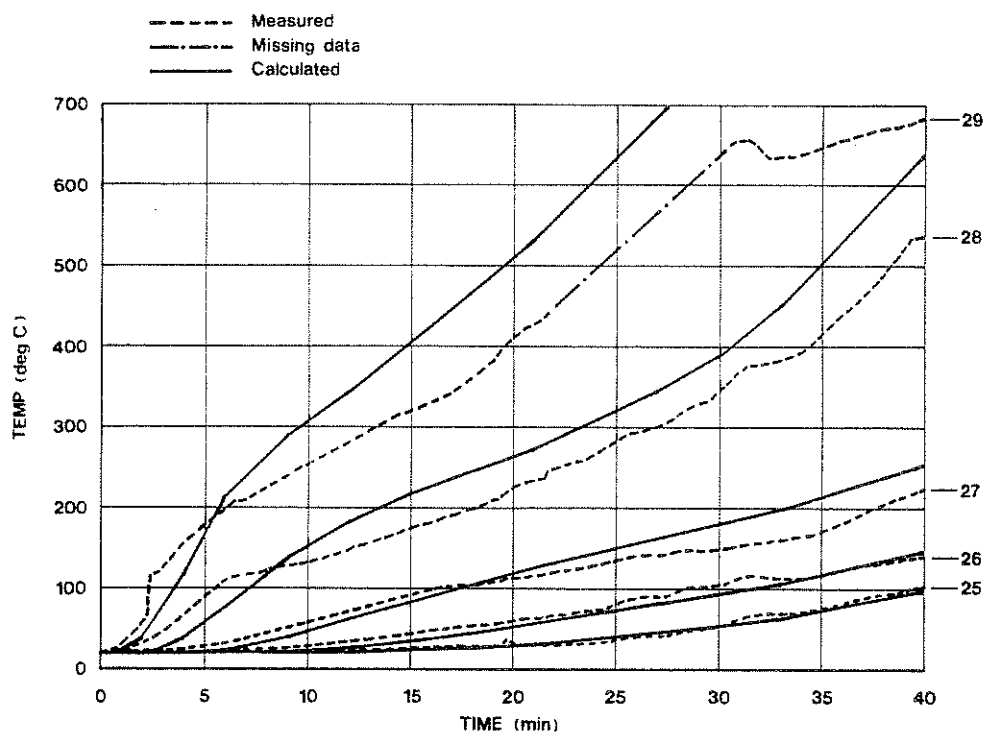


FIG. 5.8. Calculated and measured temperature fields as a function of time

The measured moisture ratios are set out in FIG. 5.7. Introduction of expressions for the moisture content in the theoretical model should produce good agreement in this case also.

FIG. 5.9 shows the penetration of the charcoal layer as a function of time. After the end of the test in the furnace, 40 minutes plus 8-1/2 minutes before the beams were extinguished, the depth of charring was measured as about 20 mm.

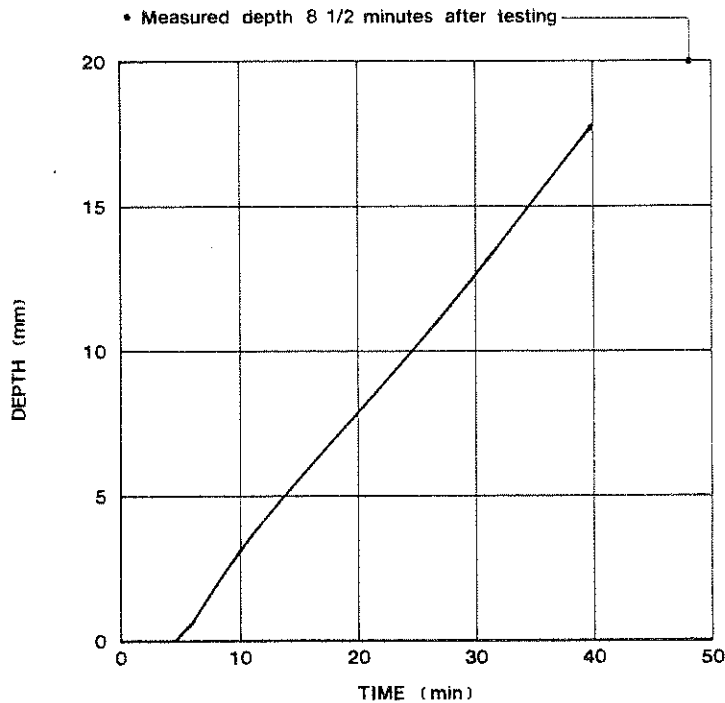


FIG. 5.9. Theoretical penetration of charcoal layer as a function of time.

5.4 Sensitivity analysis of thermal properties

In the following, the sensitivity of the charcoal layer penetration as a function of certain material data is studied. It was not the intention to carry out a full parametric study, but to test some of the parameters included in the model. The comparison is based on

the charcoal layer penetration as the dependent variable. Some of the tested material data produce quite unrealistic temperature distributions, but are nevertheless included for the sake of completeness.

The depth of charring as a function of time is set out in FIG. 5.10, the thermal conductivity being varied between $1/2 k_2$, k_2 and $2 k_2$, where $k_2 = 0.10 \text{ W/mK}$.

In the same way, FIG. 5.11 sets out the depth of charring, with the constant $\beta_1 = 1 \cdot 10^{-7} \text{ 1/s K}$ in the expression for the surface reactions being varied between $1/2 \beta_1$, β_1 and $2 \beta_1$.

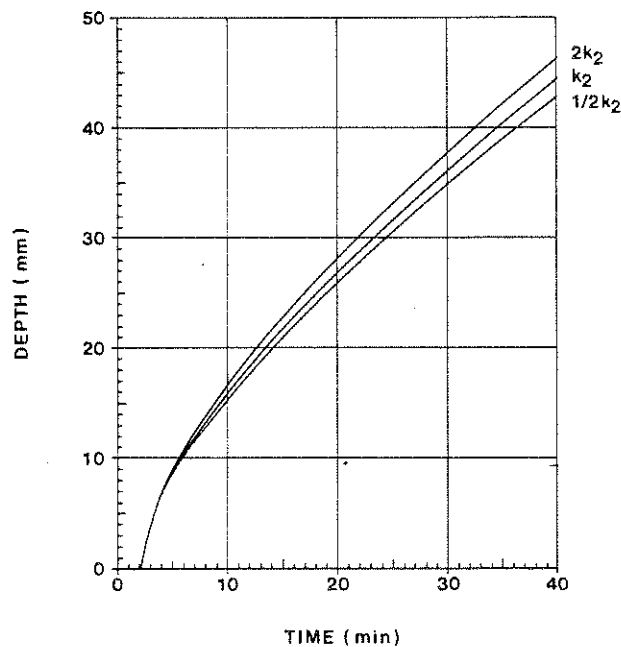


FIG. 5.10. Depth of charring as a function of time for variable thermal conductivity k_2 of charcoal. $k_2 = 0.10 \text{ W/mK}$

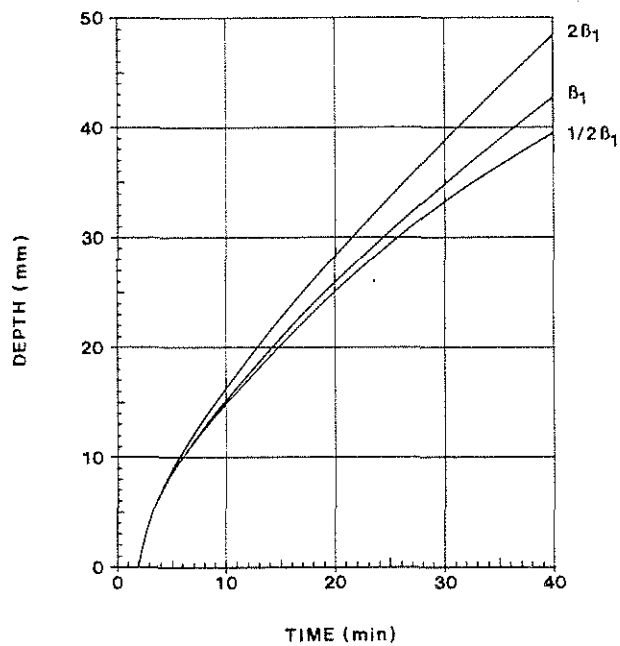


FIG. 5.11. Depth of charring as a function of time for variable rate of surface reaction according to $\dot{s} = \beta_1 T \exp(-\beta_3/T_S)$.
 $\beta_1 = 0.5 \cdot 10^{-7} \text{ 1/s K}$

If the pyrolytic reaction rate constant $b = 1500$ is halved or doubled, the curves in FIG. 5.12 are obtained.

Many authors have discussed the question of whether the pyrolytic reaction of wood is exothermic or endothermic. The significance of this for the depth of charring, when the heat of reaction Q is changed from the endothermic $+Q$ to the exothermic $-Q$, is shown in FIG. 5.13.

Other thermal properties can be tested by analytical models in the same way, but the above are among those about which there is the greatest uncertainty.

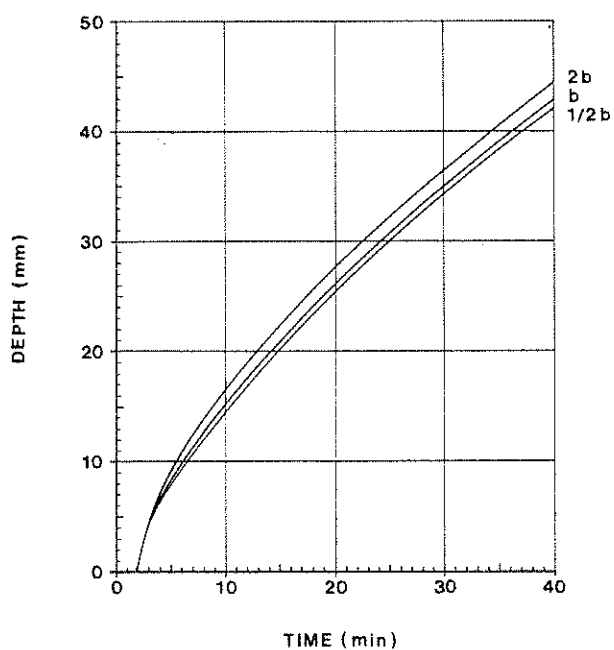


FIG. 5.12. Depth of charring as a function of time when the pyrolytic reaction rate constant b is varied in the expression $\dot{\rho} = \rho b \exp(-E_A/RT)$, $b = 1500$ 1/s.

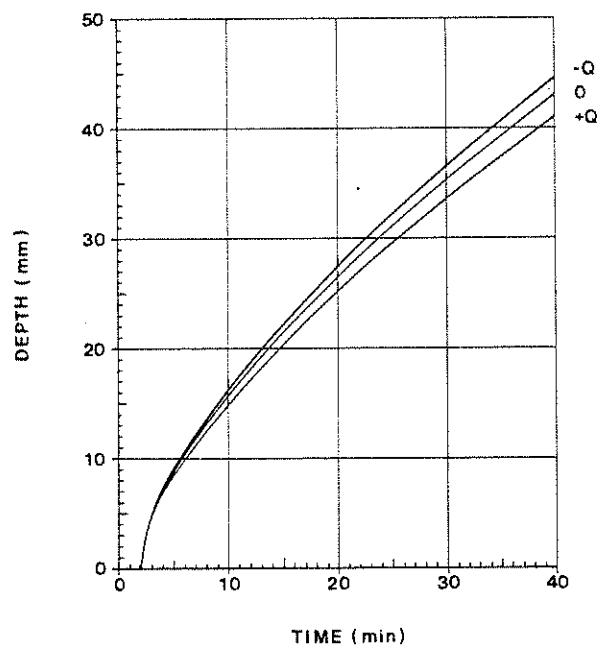


FIG. 5.13. Depth of charring as a function of time when the pyrolytic reaction is changed from an endothermic to an exothermic reaction. $Q = 125 \text{ kJ/kg}$

SUMMARY AND CONCLUSIONS

The fundamental equations for the theoretical treatment of wood during the process of pyrolysis are presented in Chapter 1. Expressions which must be specially introduced for combustible materials are those which describe the pyrolytic reaction and reactions at the surface of the material. The reactions are assumed to conform to first order Arrhenius functions. The treatment also includes the variation in heat capacity and thermal conductivity as a function of the decrease in density due to pyrolysis. When pyrolysis commences, an internal convective flow is set up which affects heat transfer both inside the material and at the surface of the material.

The numerical solution is carried out by the finite element method using the computer program WOOD1 written in FORTRAN 77. The heat balance equation is solved incrementally by the forward difference method, and the critical time increment is calculated successively for each computation stage. In view of the nature of the problem, with rapid reductions in density in the pyrolysis zone, internal convective heat flow and boundary elements which diminish in size, it is necessary to employ both small elements and short time increments in the computations.

The calculations are compared with experiments, but the paucity of well defined pyrolysis tests is evident. There is also a shortage of relevant material data, particularly at elevated temperatures, and the scatter in the reported kinetic constants is extremely large (10), (11). The comparison between calculated and measured temperature distributions shows that it is essential to take moisture content into consideration, and also that further development of the model for wet wood is important. It is evident from the

parametric study which has been carried out that the conductivity of carbon and the rate of reaction at the surface of the material have great significance for the depth of charring. It follows from this that it is important for these material properties to be better elucidated and for knowledge concerning surface reactions to be improved.

Since the computation times in these simulations were very long, it is desirable that the solution procedure should be made more efficient, especially if a two dimensional program is to be developed.

This computer program has been developed primarily as an aid in research, but, if computation times can be appreciably reduced, it can also be used for design calculations.

REFERENCES

- (1) WICKSTRÖM, U. A Computer Program for Temperature Analysis of Structures Exposed to Fire. Report No 79-2, Department of Structural Mechanics, Lund Institute of Technology, Lund 1979.
- (2) FREDLUND, B. Model for calculation of temperatures and moisture distribution and reduced cross section in timber structures exposed to fire. (In Swedish). Department of Structural Mechanics, Lund Institute of Technology, Lund 1979.
- (3) PETTERSSON, O., MAGNUSSON, S.E. and THOR, J. Fire Engineering Design of Steel Structures. Bulletin 52, Division of Structural Mechanics and Concrete Construction, Lund Institute of Technology, Lund 1976.
- (4) MUNSON, T.R. and SPINDLER, R.J. Transient Thermal Behaviour of Decomposing Materials, Part I. General Theory and Application to Convective Heating, presented at the 30th Institute of Aerospace Science Annual Meeting, New York, June 1962.
- (5) ZIENKIEWICZ, O.C. The Finite Element Method, Third Edition. McGraw-Hill, London 1977, Chapter 22.
- (6) ÖDEEN, K. Fire Resistance of Glued Laminated Timber Structures. Symposium No 3, Fire and Structural Use of Timber in Buildings, held at the Fire Research Station, Borehamwood, Herts, October 25, 1967. London 1970.
- (7) TENNING, K. Glued laminated timber beams, fire tests and experiences. (In Swedish). Symposium on the fire stability of timber structures, held at Chalmers University of Technology, Gothenburg, June 18, 1962. CTH Proceedings No 274, Gothenburg 1963.

- (8) TENNING, K. Glued Timber Beams: Fire Tests and Experience in Practice. Symposium No 3, Fire and Structural Use of Timber in Buildings, held at the Fire Research Station, Borehamwood, Herts, October 25, 1967. London, 1970.
- (9) HADVIG, S. Charring of Wood in Building Fires - Practice, Theory, Instrumentation, Measurements. Laboratory of Heating and Air Conditioning, Technical University of Denmark, Lyngby 1981.
- (10) ATREYA, A. Pyrolysis, Ignition and Fire Spread on Horizontal Surfaces of Wood. Division of Applied Sciences, Harvard University, Cambridge MA, March 1984.
- (11) FREDLUND, B. The ignition and combustion mechanism of wood. (In Swedish). Internal Report No IR79-3. Department of Structural Mechanics, Lund Institute of Technology, Lund 1979.